A Kalirin missense mutation enhances dendritic RhoA signaling and leads to regression of cortical dendritic arbors across development

Melanie J. Grubisha[a], Tao Sun[b], Leanna Eisenman[c], Susan L. Erickson[a], Shinny-yi Chou[a], Cassandra D. Helmer[a], Melody T. Trudgen[a], Ying Ding[b], Gregg E. Homanics[c,d,e], Peter Penzes[f], Zachary P. Wills[c,1], and Robert A. Sweet[a,g,1,2]

[a]Department of Psychiatry, Translational Neuroscience Program, University of Pittsburgh School of Medicine, Pittsburgh, PA 15213; [b]Department of Biostatistics, University of Pittsburgh, PA 15261; [c]Department of Neurobiology, University of Pittsburgh, Pittsburgh, PA 15261; [d]Department of Anesthesiology and Perioperative Medicine, University of Pittsburgh School of Medicine, Pittsburgh, PA 15261; [e]Department of Pharmacology and Chemical Biology, University of Pittsburgh School of Medicine, Pittsburgh, PA 15261; [f]Department of Psychiatry and Behavioral Sciences, Northwestern University Feinberg School of Medicine, Chicago, IL 60611; and [g]Department of Neurology, University of Pittsburgh School of Medicine, Pittsburgh, PA 15213

Edited by Michael E. Greenberg, Harvard Medical School, Boston, MA, and approved October 19, 2021 (received for review November 5, 2020)

Normally, dendritic size is established prior to adolescence and then remains relatively constant into adulthood due to a homeostatic balance between growth and retraction pathways. However, schizophrenia is characterized by accelerated reductions of cerebral cortex gray matter volume and onset of clinical symptoms during adolescence, with reductions in layer 3 pyramidal neuron dendritic length, complexity, and spine density identified in multiple cortical regions postmortem. Nogo receptor 1 (NGR1) activation of the GTPase RhoA is a major pathway restricting dendritic growth in the cerebral cortex. We show that the NGR1 pathway is stimulated by OMGp and requires the Rho guanine nucleotide exchange factor Kalirin-9 (KAL9). Using a genetically encoded RhoA sensor, we demonstrate that a naturally occurring missense mutation in *Kalrn*, KAL-PT, that was identified in a schizophrenia cohort, confers enhanced RhoA activitation in neuronal dendrites compared to wild-type KAL. In mice containing this missense mutation at the endogenous locus, there is an adolescent-onset reduction in dendritic length and complexity of layer 3 pyramidal neurons in the primary auditory cortex. Spine density per unit length of dendrite is unaffected. Early adult mice with these structural deficits exhibited impaired detection of short gap durations. These findings provide a neuropsychiatric model of disease capturing how a mild genetic vulnerability may interact with normal developmental processes such that pathology only emerges around adolescence. This interplay between genetic susceptibility and normal adolescent development, both of which possess inherent individual variability, may contribute to heterogeneity seen in phenotypes in human neuropsychiatric disease.

dendrite | adolescence | NGR1 | Kalirin

Schizophrenia (SZ) is a debilitating disease that affects ~1% of the population (1). Clinical symptoms, such as auditory hallucinations and delusions, emerge during the second or third decade of life. Recent studies, however, have emphasized that it is impairments in cognitive and sensory processes underlying the clinical symptoms that are the greatest contributors to functional impairment and long-term disability (2–4). Specifically, auditory processing deficits have been consistently described at the neurophysiological level and include increased threshold for detecting differences between successive auditory stimuli and decreased amplitude of the mismatch negativity response to silent gaps, processes which require an intact of the auditory cortex (5, 6). Current therapeutics have limited efficacy for cognitive and sensory function impairments and confer substantial morbidity owing to undesired side effects, underscoring the need for therapeutics targeting underlying molecular mechanisms.

Pyramidal cells (PCs) represent the most abundant neuronal type in the cerebral cortex (7), and their integrity is essential to the cognitive and sensory processes that are disrupted in SZ (5,8). Among the most consistent and highly replicated findings from human postmortem studies of SZ are reductions in dendrite length, branching, and spine density in layer 3 PCs (9). Interestingly, these deficits appear to be more reliably defined in layer 3, as layer 5 PCs have not been consistently shown to be impaired in postmortem studies of SZ (10). Because dendritic spines are the site of most excitatory synapses, much research to date has aimed to determine mechanisms of their reduction in SZ. However, total spine number is a function of both total dendrite length and spine density. Moreover, dendritic length and branching determine a PC's receptive field (11, 12), help to segment computational compartments (13), and contribute substantially to how the received signals are integrated and transmitted to the cell body (14, 15). Thus, there is a compelling need to investigate dendritic length and branching alterations in SZ.

Significance

Dendrites are long branching processes on neurons that contain small processes called spines that are the site of connections with other neurons, establishing cortical circuitry. Dendrites have long been considered stable structures, with rapid growth prior to adolescence followed by maintenance of size into adulthood. However, schizophrenia is characterized by accelerated reductions of cortical gray matter volume and onset of clinical symptoms during adolescence, with reductions in dendritic length present when examined after death. We show that dendrites retain the capacity for regression and that a mild genetic vulnerability in a regression pathway leads to onset of structural impairments in previously formed dendrites across adolescence. This suggests that targeting specific regression pathways could potentially lead to new therapeutics for schizophrenia.

Author contributions: M.J.G., S.-y.C., G.E.H., P.P., Z.P.W., and R.A.S. designed research; L.E., S.L.E., S.-y.C., C.D.H., M.T.T., and Z.P.W. performed research; Y.D., G.E.H., and Z.P.W. contributed new reagents/analytic tools; M.J.G., T.S., S.-y.C., Y.D., Z.P.W., and R.A.S. analyzed data; and M.J.G., Z.P.W., and R.A.S. wrote the paper.

The authors declare no competing interest.

This article is a PNAS Direct Submission.

[1]Z.P.W. and R.A.S. contributed equally to this work.

[2]To whom correspondence may be addressed. Email: sweetra@upmc.edu.

This article contains supporting information online at http://www.pnas.org/lookup/suppl/doi:10.1073/pnas.2022546118/-/DCSupplemental.

Published November 30, 2021.

One of the driving physiological requirements for dendritic morphogenesis is the flexibility for adjustment in development and in response to experience (16). Initial rapid growth establishes a nearly full-sized dendritic arbor prior to adolescence (17). While dendrites retain the physiological flexibility to undergo modest changes in branch points or angles to refine circuitry, the overall net arbor size remains relatively constant across adolescence and into adulthood due to a homeostatic balance between growth and retraction pathways (17, 18).

Although rapid dendritic growth is complete prior to adolescence, this developmental epoch is a particularly active period of structural changes in the brain, leading to loss of cortical gray matter volume (19–22). In SZ, this reduction in gray matter volume is accelerated (23, 24), coincident with the onset of clinical symptoms (25, 26). The predominant component of cortical gray matter is neuropil, which comprises dendrites and axonal processes (27). It is possible that accelerated gray matter reductions during adolescence in SZ may be, in part, due to regression of dendritic architecture beginning during that time. It stands to reason, then, that a genetic susceptibility in a pathway involved in dendritic morphogenesis may be further exacerbated during the adolescent transition and lead to the onset of clinical symptoms of SZ.

Among the genes found to influence dendritic morphogenesis (16, 28) is *Kalrn*. Of the multiple isoforms generated from the *Kalrn* gene through alternative splicing, the longer isoforms (KAL9 and KAL12) possess two guanine nucleotide exchange factor (GEF) domains, the second of which activates the GTPase RhoA. A missense mutation (rs143835330) coding for a proline to threonine amino acid change in the *Kalrn* gene (*Kalrn-PT*) was first identified in a resequencing analysis in individuals with SZ (29). The P→T change in *Kalrn-PT* is adjacent to the RhoA GEF domain in the KAL9 and KAL12 isoforms (29) and was shown to act as a modest gain of function for RhoA activity in a heterologous overexpression system (30). The activity of the first GEF domain, which activates Rac1, was shown to be unaltered by the *Kalrn*-PT mutation (30).

Importantly, RhoA regulation of dendritic morphogenesis requires molecular precision. Although constitutively active RhoA reduces dendritic morphogenesis in rodent PCs (31, 32), expression of dominant negative (DN) RhoA fails to affect dendritic outgrowth (33). Thus, targeting specific pathways upstream of RhoA activation is necessary to rescue structural impairments. For example, p75 is a neurotrophin receptor which directly binds to Nogo receptor (NGR) and, in response to ligand binding, subsequently activates RhoA (34, 35). In cerebellar granule neurons, the KAL9 isoform of the *Kalrn* gene has been shown to directly bind to p75 and provide the GEF domain required for RhoA activation (34). The NGR1/p75/KAL9 pathway is known to restrict neurite outgrowth (34). Specifically disrupting NGR1-mediated signaling via Nogo neutralizing antibodies promotes neurite outgrowth and extension in vitro (34, 36), and in vivo knockdown of neuronal-specific Nogo-A leads to increases in both branching and total length in Layer 2/Layer 3 (L2/3) dendrites (37). Interestingly, increased levels of Nogo messenger RNA as well as elevated levels of KAL9 protein have been described in SZ (38, 39), suggesting enhanced activity of this pathway may contribute to the impairments in dendritic morphogenesis in disease. Although to date Nogo is the most well studied, numerous myelin-associated inhibitors (MAIs) have been identified as additional NGR1 ligands and similarly serve to limit neurite outgrowth (40). Interestingly, a highly potent MAI, oligodendrocyte-myelin glycoprotein (OMGp), increases in expression across adolescence (41).

Thus, we hypothesized that *Kalrn*-PT would act as a RhoA gain of function in neurons and lead to adolescent-onset reductions in dendritic length and complexity.

Results

KAL9-PT Augments RhoA Activity in Neurons at Baseline and Following Exposure to the NGR1 Ligand OMGp. Previous work from our laboratory demonstrated that expression of *Kalrn-PT* on the KAL9 background (KAL9-PT) increased RhoA activity compared to KAL9-WT in an in vitro heterologous overexpression system (30). However, primary neuronal culture is superior in that it captures features of normal neuronal development and endogenous kalirin expression, features lacking in heterologous systems. Thus, we derived cortical neuronal cultures from E18 rats and overexpressed either KAL9-wildtype (WT) or KAL9-PT at equivalent levels ($P = 0.26$ between genotypes, *SI Appendix*, Fig. S1). At the time of transfection with the Kalirin-containing plasmids, neurons were also transfected with a fluorescence resonance energy transfer (FRET)-based genetically encoded RhoA sensor (RhoA2G) (42). As previously described (43), regions of interest (ROIs; 5- to 10-μm boxes) were defined along the dendritic shaft and soma, affording the ability to determine RhoA activation with subcellular localization. Baseline RhoA activity was recorded over 5 min and an average value for each ROI calculated. To determine if RhoA is activated downstream of OMGp, following this 5-min baseline imaging, neurons were exposed to OMGp peptide (1ng/μL; R&D Systems), after which neurons were continually imaged for a subsequent 15 min.

Representative neurons indicated (white hatched boxes) are shown in Fig. 1 *A* and *D*, with activity represented as a heat map. While overexpression of KAL9-WT showed no increase in baseline RhoA activity in dendrites compared to controls, KAL9-PT increased RhoA activity relative to KAL9-WT or controls (Fig. 1*C*), with differences observed in midproximal ROIs along the dendritic shaft (Fig. 1*B*).

In experiments where neurons were exposed to OMGp (Fig. 1 *D–F*), we observed a significant increase in RhoA activation in proximal dendritic ROIs over baseline in all groups, as illustrated by a time course tracking the 1-min mean ΔF/F RhoA activity (Fig. 1*E*) or a summary graph of the 1-min maximum ΔF/F RhoA activity of neurons under indicated conditions (Fig. 1*F*). Furthermore, neurons expressing KAL9-PT showed an enhanced response to OMGp relative to KAL9-WT (Fig. 1*D*). Note, no significant change in soma area (GFP only = 190.91 ± 9.89 μm^2; KAL9-WT = 201.67 ± 13.68 μm^2; KAL9-PT = 205.89 ± 9.96 μm^2; $P = 0.63$) or soma perimeter (GFP only = 52.15 ± 1.2 μm; KAL9-WT = 54.43 ± 2.25 μm; KAL9-PT = 53.42 ± 1.16 μm; $P = 0.62$) was observed in neurons expressing either Kal9 construct ($n = 10$ neurons).

OMGp Signaling in Pyramidal Neurons Limits Dendritic Arborization via an NGR1- and KAL9-Dependent Pathway. In cerebellar granule neurons, KAL9 mediates GEF activation of RhoA downstream of NGR/p75 signaling (34). This serves to limit early neurite outgrowth. We hypothesized that in excitatory pyramidal neurons, KAL9 might also regulate RhoA signaling downstream of NGR1 signaling via this same pathway. We further hypothesized that in pyramidal neurons, this pathway may act on dendritic arbors. To test this, we first utilized hippocampal slice culture, as the role of NGR1 in reducing dendritic arbor size has been well characterized in this system (44). We overexpressed NGR1 in CA1 PCs and observed decreased dendritic length and complexity compared to GFP-only control, as previously described. Concomitant transfection with a previously validated short-hairpin RNA directed at KAL9 (34) (see also *SI Appendix*, Fig. S2 for evidence of effective knockdown) rescued this phenotype, suggesting that KAL9 is required for NGR1 signaling to restrict dendritic growth (Fig. 2).

NGR1 is known to signal through multiple pathways, thus we conducted a second series of experiments to further define

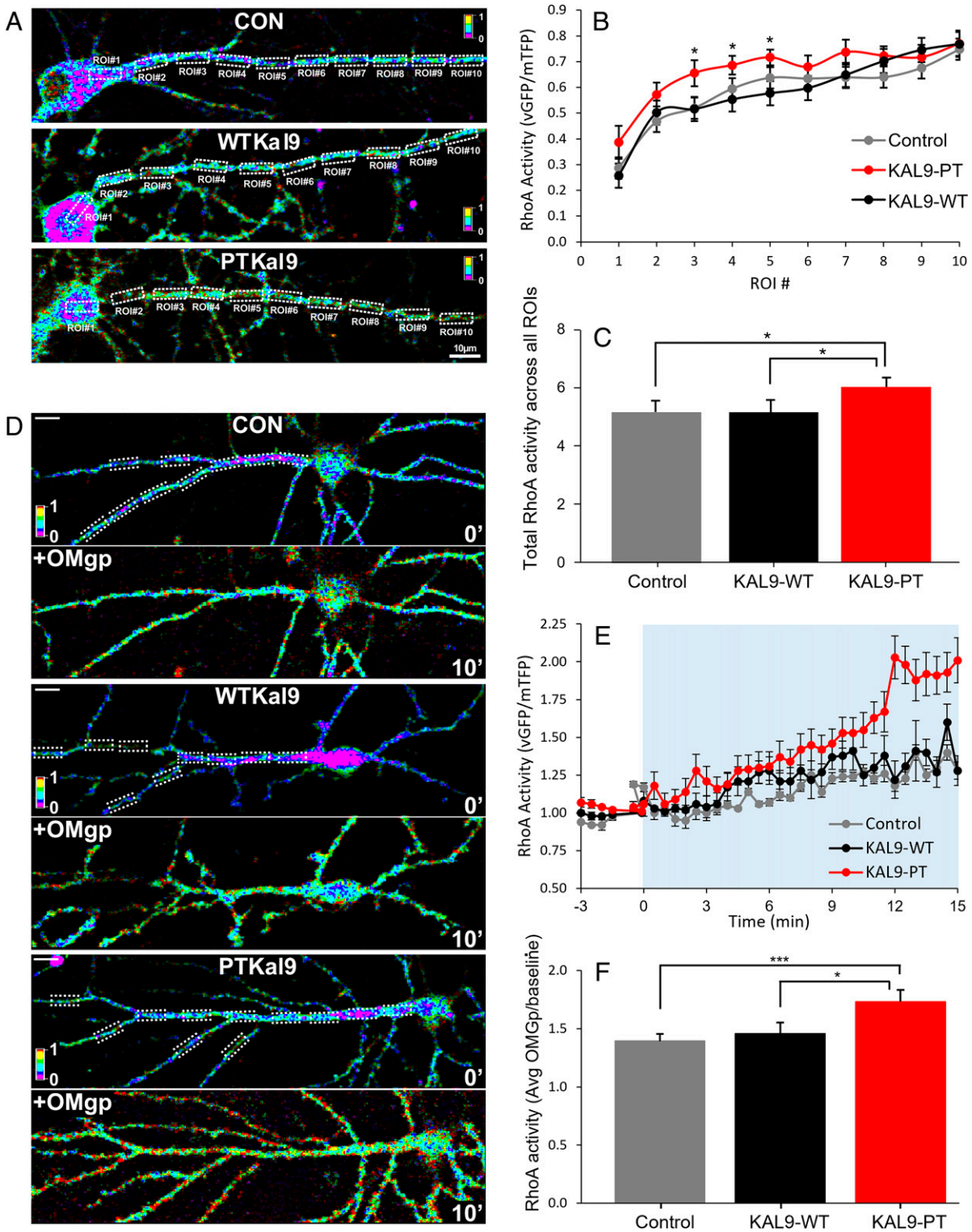

Fig. 1. KAL-PT confers gain of function for RhoA activity in primary neurons. (*A*) Representative images of RhoA sensor activity as measured by FRET imaging in neurons control, KAL9-WT, and KAL9-PT transfected with indicated Kal9 plasmids neurons (transfected at DIV8, imaged at DIV14 to 18). ROIs are indicated by dashed white boxes, with 1 ROI within the soma and 2 to 10 defined along the dendritic shaft. Activity is represented as a heat map, with warmer colors indicating increased activity. (*B*) KAL9-PT shows increased RhoA sensor activity in proximal dendritic shaft ROIs (*$P < 0.05$ versus KAL-WT). $n = 11$ to 15 neurons per condition. (*C*) The average RhoA activity across proximal ROIs (1–5)/neuron shows a significant increase in RhoA activity in KAL-PT compared to control and KAL-WT. $n = 13$ to 15 neurons per condition. Data shown are ± SEM*$P < 0.04$. (*D*) Representative images of RhoA sensor activity as measured by FRET imaging in neurons expressing indicated Kal9 plasmids at baseline (*Top*) and in response to OMGp exposure (*Bottom*) at indicated timepoints. (*E*) Graph of the average ΔF/F RhoA activity (F = 0 to 5 min average of all ROIs) of indicated ROIs/conditions from representative images (*D*, *Top*) over indicated time course following OMGp addition (1 ng/μL, indicated by light blue shading). (*F*) The 1-min max ΔF/F RhoA activity for all ROIs of indicated conditions following OMGp addition. $n = 15$ to 28 neurons per condition (four to six proximal shaft ROIs per neuron). Data shown are ± SEM ***$P < 0.0001$, *$P < 0.03$. (Scale bar, 10 μm.)

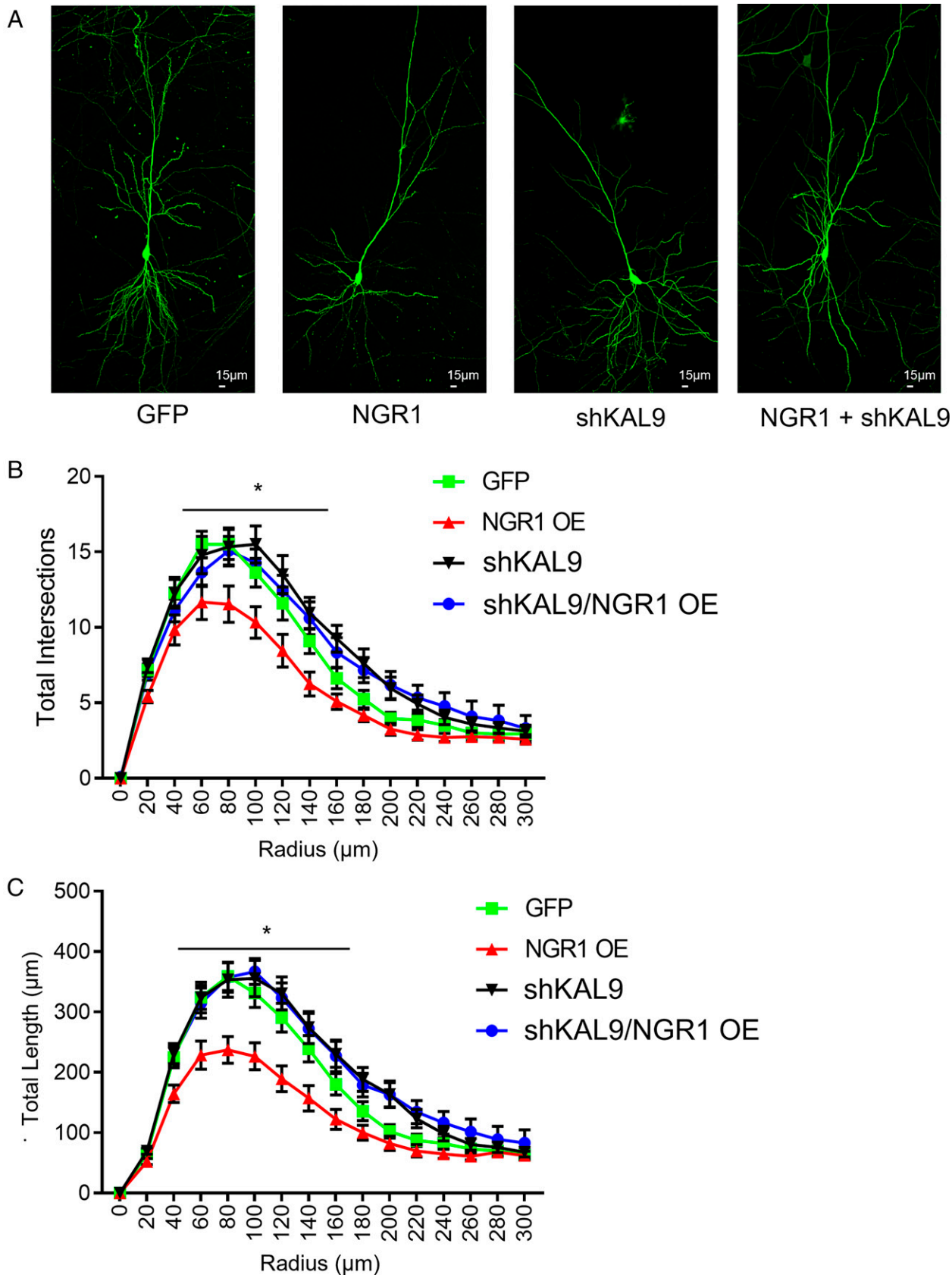

Fig. 2. KAL9 is necessary for NGR1-mediated dendritic growth restriction. (*A*) Representative images of CA1 pyramidal neurons expressing GFP ± NGR1 or shKAL9. (*B*) Sholl analysis of total intersections shows a decrease in dendritic complexity with NGR1 overexpression (*$P = 0.03$) that is rescued by concomitant transfection with shKAL9. (*C*) Sholl analysis of total length shows a decrease in dendritic length with NGR1 overexpression (*$P = 0.01$) that is rescued by concomitant transfection with shKAL9. $n = 20$ to 24 neurons per condition from three independent experiments. Data shown are ± SEM.

the role of KAL9 in mediating NGR1-dependent effects on dendritic architecture. To do this, we used the MAI, OMGp, which has previously been shown to act through NGR1 to inhibit early neurite outgrowth (45). However, OMGp has been observed to be abundantly expressed by adult central nervous system neurons where its role remains unknown (46). Thus, we hypothesized that OMGp would signal through the NGR1 and require KAL9 to restrict dendritic arborization in pyramidal neurons (Fig. 3*A*). Treatment of dissociated cortical neurons (48-h treatment from day-in-vitro (DIV)12 to 14) with OMGp (200 ng) leads to reductions in both length ($P < 0.0001$) and complexity ($P < 0.0001$) of dendritic arbors (Fig. 3 *B* and *C*), suggesting a potential role for this protein in regulating dendritic architecture. We next genetically ablated NGR1 (*SI Appendix*, Fig. S2) using a previously validated shRNA construct (44) and found that knockdown of NGR1 expression mitigates the effect of OMGp on dendritic architecture (Fig. 3 *D* and *E*). This suggests OMGp functions via the NGR1 signaling pathway to inhibit dendrite growth. Finally, we genetically ablated KAL9 expression (*SI Appendix*, Fig. S2) through use of a validated shKAL9 construct (34) and also observed OMGp failed to produce a significant effect on dendritic architecture in the absence of KAL9 (Fig. 3 *F* and *G*). Pharmacologic inhibition of RhoA with the commercially available RhoA inhibitor CT04 prevents the OMGp-induced phenotype, suggesting that RhoA activation is a necessary downstream mechanism (*SI Appendix*, Fig. S4). Taken together, these findings demonstrate OMGp can restrict dendritic length and complexity in cortical neurons, and this effect requires both NGR1 and KAL9 and involves downstream RhoA activation.

Given the increased RhoA activity downstream of KAL9-PT, we next sought to determine if the effect of OMGp signaling on dendrites via NGR1/p75/KAL9 was enhanced by KAL9-PT compared to wild type. To test this, we transfected dissociated cortical cultures with either KAL9-WT or KAL9-PT on DIV8, then stimulated with either phosphate buffered saline alone or 200 ng OMGp for 48 h on DIV12 to 14. Neurons were fixed, and dendritic arbors were reconstructed. As Fig. 3 shows, OMGp significantly decreased both length and complexity of dendritic arbors in both KAL9 genotypes. This effect was more pronounced in the KAL9-PT neurons versus KAL9-WT [$P = 0.012$ between KAL9-WT (+) OMGp and KAL9-PT (+) OMGp for dendritic length; $P = 0.01$ between KAL9-WT (+) OMGp and KAL9-PT (+) OMGp for dendritic intersections], suggesting KAL9-PT enhances NGR1-RhoA signaling resulting in more pronounced dendritic growth deficits (reference *SI Appendix*, Fig. S3 for representative images across conditions).

***Kalrn-PT* Mice as a Model of the P→T Missense Mutation.** To determine the impact of the *Kalrn*-PT mutation in vivo and preserve the physiologic stoichiometry of kalirin, we introduced the missense mutation at the endogenous locus of the C57BL/6J mouse strain using CRISPR/Cas9 gene editing technology. We designed a custom targeted single guide RNA (sgRNA94) and a repair oligonucleotide containing the C→A missense mutation constituting *Kalrn-PT* (*SI Appendix*, Table S1 and *Supplemental Methods*). In addition to the missense mutation, a silent mutation located in the third base pair of the codon harboring the missense mutation was introduced (C→T). This silent mutation produced a unique restriction site for Hinf1. Thus, restriction digest could be used for rapid and reliable genotyping assays once the line was established.

A founder male mouse who was homozygous for the *Kalrn-PT* mutation was chosen for line establishment (*SI Appendix*, Fig S5). Confirmatory Sanger sequencing was performed to verify presence of both the missense and silent mutations in the correct region. To confirm absence of any unintended off-target effects, we used prediction software to generate 18 sites with high homology to our guide sequence. Our founder mouse was confirmed to be free of off-target effects at all sites tested by both PCR and Sanger sequencing (*SI Appendix*, Table S2 and *Supplemental Methods*). To establish the *Kalrn-PT* line, we bred our founder mouse with a purchased wild-type female of the C57BL/6J strain. Although the founder mouse was confirmed to be homozygous for the *Kalrn-PT* mutation, this was assessed only in peripheral cells derived from a tail snip sample and did not account for any mosaicism that exists in the gametes. Knock-in mice are known to possess mosaicism (47), thus we monitored the rate of mutation transmission in the F1 generation as well as performed Sanger sequencing to confirm genotypes in all F1 generation derived from the founder mouse. It was determined that our founder mouse was transmitting the *Kalrn-PT* mutation with ~50% efficiency, and all F1 offspring retained for the line were confirmed to have only the missense and silent mutations at the desired locus. Subsequent generations were determined to be transmitting the mutation at expected Mendelian ratios.

We next evaluated whether the *Kalrn-PT* mutation was associated with altered levels of *Kalrn* mRNA and protein. Kalirin isoform expression is known to be developmentally dependent, with isoforms 9 and 12 being the predominate isoforms for the first 2 wk of age before kalirin-7 expression increases and becomes the dominant isoform (48, 49). Our assays were performed on postnatal day 28 to 35 animals, an age at which Kalirin-7 would be expected to be the most abundant isoform. We performed quantitative real-time PCR using primers specific for the three most abundant kalirin isoforms, specifically Kalirin-7,-9, and-12. There was no influence of genotype on the expression levels of any of the major Kalirin isoforms. Given recent data that demonstrate an increased frequency of exon skipping in Kalirin (exon 36) associated with SZ (50), we also examined if there was any impact of the *Kalrn-PT* mutation on increased frequency of this naturally occurring splice variant. There was no change in the relative expression of this variant as a result of genotype. Importantly, there was no change in transcript expression levels of the affected isoforms (i.e., Kalirin-9 and -12), and there was no compensatory change in expression levels of Kalirin-7. We further confirmed endogenous levels by evaluating the protein expression by Western blot. Again, there was no change in levels of any of the major Kalirin isoforms as a result of genotype (*SI Appendix*, Fig S5).

Dendritic Morphogenesis Is Impaired in *Kalrn-PT* Mice In Vivo. Abnormalities in sensory processing (5) as well as reductions in PC somal size (51), spine density (52), and neuropil (53) have all been described in SZ. These functional and structural deficits implicate impairments in layer 3 of primary auditory cortex (A1) (8). Thus, we initially chose to focus on layer 3 PCs in A1 to test the effects of *Kalrn-PT* on dendritic morphology (*SI Appendix*, Fig. S6). We generated a cohort of 12-wk ± 3 d mice and used Golgi–Cox staining to detail neuronal structure. A total of five animals/genotype/sex were included, and vaginal cytology on female animals was collected at time of killing. Based on pilot studies, the variabilities across neurons from the same layer and region within animal were found to be quite small. We thus chose six neurons per animal for imaging and reconstruction. While our sample size was underpowered to detect primary effects of sex, our groups were balanced for sex across genotypes, ensuring that we did not introduce systematic bias. We did nonetheless test the effect of sex in our small sample size to ensure that there was no significant effect of sex on any of the dendritic measures in our cohort (*SI Appendix*, Table S3), and thus the groups were combined to provide a total of 10 wild-type and 10 *Kalrn-PT* homozygous animals. Using Sholl analysis, we found significant reductions in dendritic length and complexity across both the apical (Fig. 4 *C* and *D*) and basilar

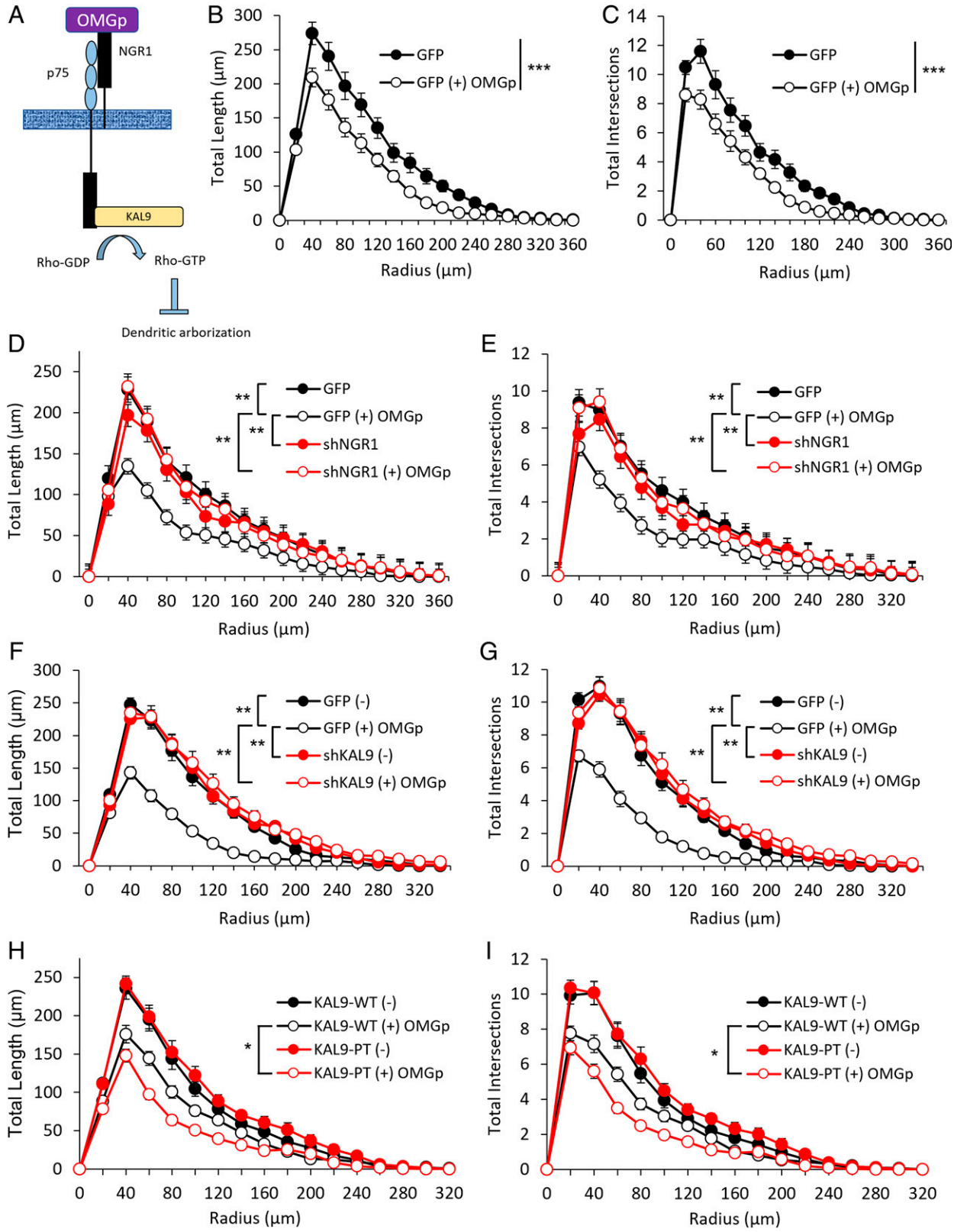

Fig. 3. Dendritic growth restriction by OMGp requires both NGR1 and KAL9. (*A*) Schematic of the OMGp-NGR1/p75/KAL9 pathway that impedes dendritic arborization. (*B*) OMGp (200 ng, 48h) treatment of DIV12 to 14 cortical neurons reduces total dendritic length (*C*) and complexity. (*D*) Genetic ablation of NGR1 expression mitigates the effect of OMGp treatment on dendritic length (*E*) and complexity in cortical neurons. (*F*) Genetic ablation of KAL9 expression mitigates the effect of OMGp treatment on dendritic length (*G*) and complexity in cortical neurons. Overexpression of KAL9-PT shows further reductions in dendritic (*H*) length and (*I*) complexity in response to OMGp treatment compared to overexpression of KAL9-WT. $n = 26$ to 30 total neurons per condition from three independent experiments; data were averaged within experiment and experiment used as biological replicate. Data shown are ± SEM $^{***}P < 0.0001$, $^{**}P < 0.01$, $^{*}P < 0.05$.

(Fig. 4 *E* and *F*) arbors ($P = 0.0002$ and $P < 0.0001$, respectively). Representative reconstructions are shown in Fig. 4 *A* and *B*. In contrast to layer 3 PCs, those found in layer 5 have not been consistently shown to be impaired in postmortem studies of SZ (10). Using the same approach as described above, we found that there was no significant difference in dendritic length or complexity in layer 5 PCs between genotypes (*SI Appendix*, Fig. S7).

In addition to reductions in dendritic length and complexity in L3 PCs in SZ, human postmortem studies consistently demonstrate reduced L3 dendritic spine number and spine density per unit of tissue in A1 in SZ (9, 54). To determine if dendritic spine density was also altered in *Kalrn-PT* mice, we used the Golgi material generated from our 12-wk cohort described above. We added an additional animal per genotype in order to balance estrus phase across female animals (two animals/phase/genotype from three phases: estrus, metestrus, proestrus; *SI Appendix*, Table S3*A*). Balancing estrus phase across groups ensured we did not introduce any systematic bias, and previous work in rodent cortex has shown that steady-state cortical spine density does not differ across estrus phase (55). Nonetheless, we did evaluate estrus phase as a potential covariate despite our small sample size and found no significant effect (*SI Appendix*, Table S3*B*), consistent with the literature. Fig. 5 *A* and *B* shows a representative image of a PC containing a secondary apical dendrite along which spines were manually counted, along with representative images from *Kalrn-WT* (*Top*) and *Kalrn-PT* (*Bottom*) mice. Quantitative data are shown in Fig. 5*C*, demonstrating no mean difference in spine density per unit dendrite length across genotypes ($P = 0.73$). However, spine number and spine density per unit of tissue are a function of both total dendritic length and spine density per unit length. Previous work has shown that colocalization of spinophilin and phalloidin can be used to identify dendritic spines (9, 56–59). As shown in Fig. 5 *D* and *E*, we found a reduction in tissue density of immunoreactive puncta dual labeled for spinophilin and phalloidin in *Kalrn*-PT mice compared to *Kalrn*-WT ($P = 0.05$). Furthermore, given the reductions in dendritic length and complexity, we also tested if total gray matter volume reductions were present. Volume measurements performed on the neocortex of a small cohort of 12-wk-old mice showed a 4% reduction in gray matter volume, though this did not achieve statistical significance ($P = 0.24$, *SI Appendix*, Fig. S8).

***Kalrn*-PT Mice Exhibit Increased Gap Duration Threshold.** To test if the structural deficits observed in auditory cortex L3 PCs were associated with functional impairments, we sought to test cortical auditory function in a 12-wk cohort of wild-type and *Kalrn*-PT mice. We used the acoustic startle response paradigm in which the extent of response inhibition by a prepulse (prepulse inhibition, PPI) is quantified. When the prepulse is a noise at a lower sound-level pressure than the startle-eliciting noise (noise-PPI), PPI is dependent upon subcortical auditory processing (60). Conversely, detection of silent gaps embedded in noise has been shown to require the primary auditory cortex (61, 62). If the animal detects the gap, the startle response is inhibited. Thus, use of a modified PPI paradigm in which the prepulse is a silent gap (Gap-PPI) can be used to assess the integrity of the auditory cortex.

We generated a cohort of male and female mice, aged 12 wk ($n = 11$ *Kalrn*-WT, $n = 12$ *Kalrn*-PT), and tested them for baseline acoustic startle response, noise-PPI, and Gap-PPI (*SI Appendix*, Fig S9). We established that there is no significant difference in baseline acoustic startle response between genotypes (*Kalrn*-WT = 0.435 ± 0.049N, *Kalrn*-PT = 0.339 ± 0.041N, $P = 0.15$). Noise-PPI is similarly equivalent between genotypes, suggesting that subcortical auditory processing is unaffected by the *Kalrn*-PT mutation. To assess cortical auditory processing, we examined thresholds for Gap-PPI, defined as the shortest gap durations to elicit significant PPI. The threshold for Gap-PPI increased from 4 ms in *Kalrn*-WT mice to 20 ms in the *Kalrn*-PT mice (*SI Appendix*, Fig S9, thresholds indicated by arrows). Taken together, these results suggest that, compared with *Kalrn*-WT mice, the *Kalrn*-PT mice exhibit decreased detection of gap in noise at shorter gap durations.

***Kalrn-PT* Exerts Effects across Development.** Despite onset of clinical symptoms being delayed until late adolescence/early adulthood, SZ is considered a neurodevelopmental disease. The neurodevelopmental hypothesis of SZ has received support from recent research that implicates shared genetic risk with other syndromes typically considered "neurodevelopmental disorders" with childhood onset (autism spectrum disorder, intellectual disability), and the high degree of comorbidity suggests an underlying pathology for SZ that targets early brain development (63). Dendritic arborization is known to occur early in development, with arbors reaching near adult size by P21 in mice, and subsequent changes acting primarily to refine circuitry (64, 65). Thus, to determine if the dendritic impairment observed in the 12-wk cohort arose early in development, we generated a cohort of 4-wk ± 3 d mice. Six neurons/animal were imaged and manually reconstructed in NeuroLucida, and a total of five animals/sex/genotype were included (*SI Appendix*, Fig S11). Similar to the 12-wk cohort, there was no effect of sex on any of the dendritic measures, and thus the sexes were combined to provide 10 animals/genotype in the final analyses. We analyzed the age effect within genotypes and found a significant genotype*age interaction for both length and intersections. Specifically, basilar dendritic length (Fig. 6*C*) and complexity (Fig. 6*A*) remained stable across development within *Kalrn-WT* mice. Conversely, there is a regression in basilar arbor length (Fig. 6*C*) and complexity (Fig. 6*A*) within *Kalrn-PT* mice across development. In contrast, apical arbors exhibit modest continued growth across adolescent development (Fig. 6 *B* and *D*), consistent with previous reports of L3 PCs across adolescence in rodents (26). In *Kalrn*-PT mice, however, the arbors remain static in length and complexity across adolescence (Fig. 6 *B* and *D*). Sholl analyses for each parameter measured within genotype across ages are shown in *SI Appendix*, Fig. S10.

Discussion

We hypothesized that the *Kalrn*-PT mutation expressed in KAL9 (KAL9-PT) would increase baseline RhoA activity in neurons, specifically within the subcellular distribution consistent with the protein's normal expression. We further hypothesized that this activity would be downstream of NGR1 signaling and have functional effects on dendritic morphology. Using genetically encoded RhoA sensors, we find increased RhoA activity, both baseline and in response to OMGp stimulation, in the proximal dendritic shaft in cortical neurons overexpressing KAL9-PT. We further found that genetic knockdown of KAL9 mitigates the structural impairment seen in dendrites due to NGR1 overexpression. We demonstrated that OMGp acts via NGR1 in PCs to restrict dendritic length and complexity, an effect which requires KAL9 and is enhanced by KAL9-PT. OMGp stimulation increases RhoA activation in the dendrite, and inhibition of RhoA activation blocks the effect of OMGp stimulation on dendritic architecture. In a genetic mouse model of the *Kalrn*-PT mutation, we found impairments in dendritic morphology of L3 pyramidal neurons in auditory cortex that resulted from dendritic arbor regression across adolescence. These dendritic structural impairments occur in the absence of changes in spine density per unit of dendrite length, while notably inducing a modest reduction in tissue density of presumptive spines as measured by spinophilin/phalloidin dual-reactive puncta. Finally, we show that early adult *Kalrn*-PT mice demonstrate an impaired auditory gap detection threshold.

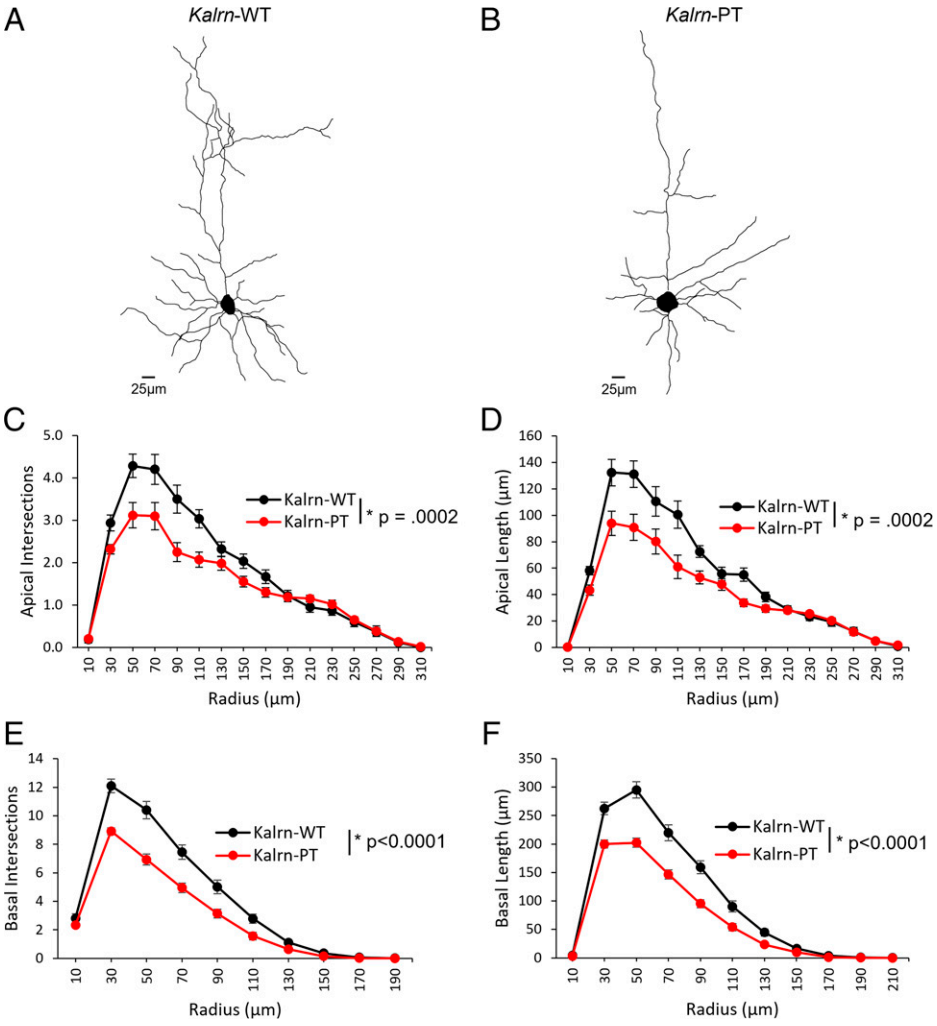

Fig. 4. *Kalrn*-PT leads to reductions in dendritic architecture at 12 wk. Dendritic reconstructions from Golgi-stained PCs in A1 of 12-wk-old (*A*) *Kalrn*-WT and (*B*) *Kalrn-PT* mice demonstrate reduced dendritic complexity and length in (*C* and *D*) apical arbors as well as (*E* and *F*) basilar arbors. (n = 10 mice per genotype, 6 neurons per animal.) Results shown are from repeated-measures ANOVA with main effect of genotype. *P* values for each analysis are indicated within the corresponding graph. Data shown are average values across animals ± SEM. All data used in these analyses are available in Datasets S1–S4.

KAL9 as a Spatially Restricted RhoGEF. *Kalrn* belongs to a conserved family of proteins that possess GEF domains. The KAL9 isoform, a dual GEF containing two active domains, is largely excluded from dendritic spines (30), instead localizing primarily to the dendritic shaft. This distinct subcellular localization suggests it tightly regulates RhoA activity within a specific microdomain within the neuron. KAL9 likely exerts its effects primarily through cytoskeletal rearrangements within the dendrites. Our findings in neurons support the notion that KAL9 regulates RhoA activity in dendrites, as we see increased baseline RhoA activity in the proximal shaft, but not soma, of neurons overexpressing KAL9-PT. While OMGp stimulation increases RhoA activation above baseline across all conditions, we see a significantly increased response in RhoA activation following OMGp stimulation in neurons overexpressing KAL9-PT compared to either control or KAL9-WT alone. Importantly, we do not see a significant difference in RhoA activation downstream of OMGp between KAL9-WT overexpression compared to control, suggesting that the stoichiometry is likely limited by NGR1 availability and the enhancement in RhoA activation seen with KAL9-PT results from increased GEF activity per molecule of KAL9.

The role of RhoA activation in dendritic biology is complex. Although constitutively active RhoA reduces dendritic morphogenesis in rodent PCs (31, 32), expression of DN RhoA fails to affect dendritic outgrowth during development (33). These finding suggest RhoA activity may be significantly restricted during dendritic development, and modulation of specific effectors is required to block its activity. Previous work in cerebellar granule neurons identified KAL9 as a critical component of the NGR1/p75 signaling pathway, with KAL9 being responsible for activation of RhoA in neurites (34). However, given NGR1's numerous signaling mediators in different cell types in the brain (37), we sought to determine if KAL9 regulated NGR1 specifically in pyramidal neurons. To test this, we performed a series of experiments involving both overexpression as well as genetic knockdown approaches. The effect of NGR1 overexpression on dendritic morphology in CA1 hippocampal pyramidal neurons has been extensively characterized (44), allowing us to utilize this system to test if KAL9 is necessary to mediate NGR1's effects. We show that KAL9 is necessary for the effect of NGR1 overexpression on dendritic architecture in CA1 pyramidal neurons, as genetic knockdown of KAL9 rescues the structural impairments induced by NGR1 overexpression. Next, we demonstrate that the MAI OMGp acts as a ligand for NGR1 to restrict dendritic length and complexity. OMGp's inhibition of dendritic growth is reversed by genetic ablation of KAL9, suggesting KAL9 is required for OMGp's effects on dendritic architecture. Interestingly, KAL9-PT enhances OMGp's inhibition of dendritic growth. While KAL9 likely signals through numerous pathways (66), it is unlikely that an orthogonal pathway or an off-target effect of the shRNA used is responsible for these findings as genetic ablation of KAL9 alone does not cause a significant change in dendritic architecture compared to control. Taken together with our findings of increased RhoA activation downstream of OMGp stimulation, this suggests that KAL9-PT enhances OMGp's effect on dendrites through an RhoA-dependent mechanism.

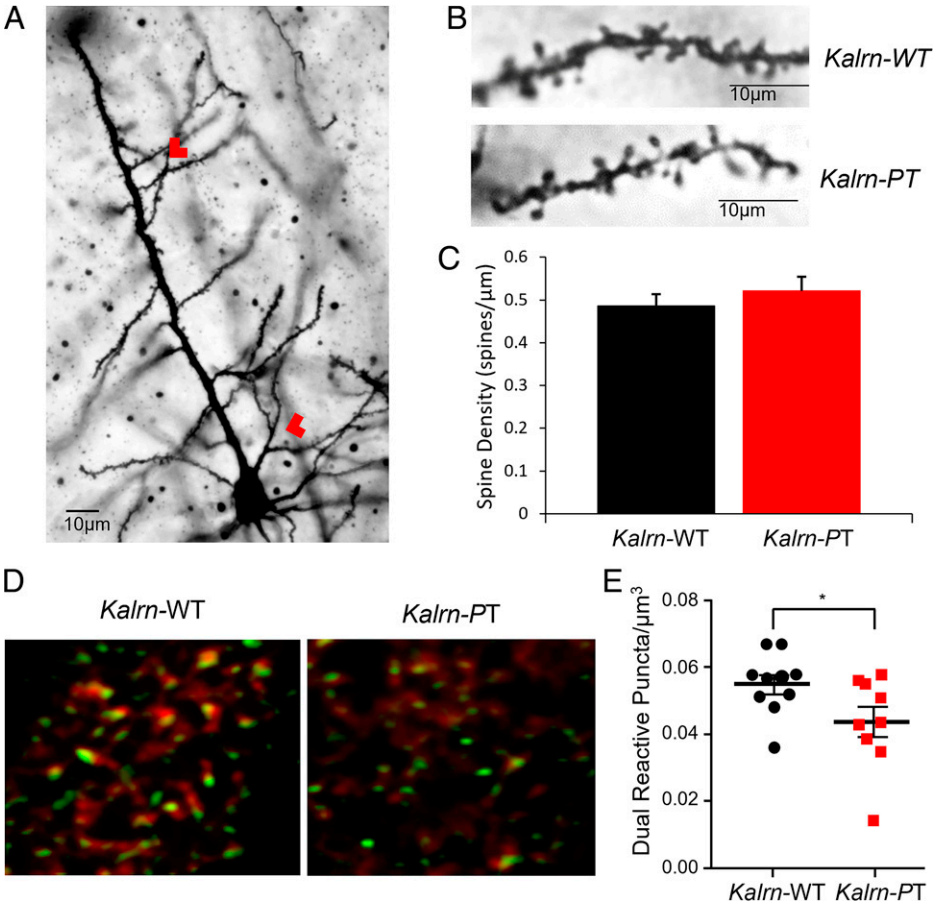

Fig. 5. *Kalrn*-PT does not reduce dendritic spine density per unit length of dendrite compared to *Kalrn*-WT. (*A*) Representative Golgi image of a PC imaged for spine density analysis. Red arrowheads indicate designated length along primary apical dendrite wherein any secondary arising within that area was included for density analysis. (*B*) Representative images of dendritic segments on which spines were counted (*Kalrn-WT* image shows 0.49 spines/μm, *Kalrn-PT* image shows 0.51 spines/μm). (*C*) No change in spine density was observed as a result of genotype (*Kalrn-WT* average 0.49 spines/μm, *Kalrn-PT* average 0.52 spines/μm; $P = 0.73$; $n = 10$ animals/genotype). (*D*) Colocalization of phalloidin-labeled (red) and spinophilin-immunoreactive (green) puncta in layer 3 of A1 from *Kalrn-WT* and *Kalrn-PT* mice ($n = 10$ animals per genotype). In total, 10 sites per animal were imaged. Representative images for each genotype are shown. (*E*) Data shown are number of dual-reactive puncta/μm^3 of tissue for each animal. There is a decrease in dual-labeled puncta in the *Kalrn-PT* mice compared to WT (*$P = 0.05$). All data shown are ± SEM.

Dual GEFs and Neuropsychiatric Disease. Rho GTPases have emerged as key regulators of dendritic morphogenesis and, not surprisingly, are increasingly found to be associated with neuropsychiatric diseases whose pathology includes abnormal dendritic architecture. For example, a large proportion of genes implicated in intellectual disability encode small GTPases (67, 68). More recent evidence further suggests that disruptions in regulators of small GTPase activity, namely dual GEFs, are associated with human neurodevelopmental diseases. A hotspot of de novo mutations in Trio, a dual-GEF paralog of KAL9, was recently described in autism spectrum disorder (69). An exome-wide significant enrichment in Trio loss-of-function mutations has also more recently been described in SZ (https://schema.broadinstitute.org/gene/ENSG00000038382). *KALRN* itself has been implicated in multiple neuropsychiatric diseases, perhaps most notably SZ (70). The *KALRN*-PT mutation was initially discovered in a resequencing analysis of a SZ cohort, conferring an OR > 2 (29). More recently published evidence found a transcriptome-wide increase in exon skipping in *KALRN* transcripts in SZ (50). The exon skipped at a greater rate in SZ was exon 36, present only in the dual-GEF isoforms, KAL9 and KAL12. The increasing body of evidence implicating dual GEFs in human neurodevelopmental disease, in particular SZ, underscores the potential importance of tightly regulating small GTPase activity with precise spatial and temporal resolution.

Dendrites in Disease and Development. A consistent feature across the above mentioned neurodevelopmental disorders (see *Dual GEFs and Neuropsychiatric Disease*), most notably SZ, is impaired dendritic architecture. Specifically, reductions in both dendritic spine number and density as well as dendritic length are among the most reproducible findings in postmortem studies of SZ (10). Since dendrites are a principal component of cortical gray matter, it is possible that their reduction in SZ is a contributing factor to the observed reductions in gray matter volumes in disease. Importantly, baseline gray matter volumes are not reduced in clinical high-risk groups between those that will later go on to develop SZ and those that will remit (71–73). Instead, the reductions emerge during adolescence and young adulthood concurrent with the transition to symptomatic illness.

Thus, understanding molecular mechanisms leading to impairments of dendritic growth, development, and maintenance in SZ requires developmental context. While overexpression and knockdown models are powerful tools in allowing us to understand the basic biology of molecules with respect to active domains, signaling pathways, etc., they fail to recapitulate normal developmental patterning and physiologic levels of expression. CRISPR/Cas9 affords the ability to selectively edit the genome with high precision, including inserting single base pair mutations at a specific locus (74, 75). Thus, we employed this modality to generate a mouse line containing the *Kalrn*-PT missense mutation at the endogenous locus to better study the effects of modest gain-of-function RhoA activity in *Kalrn* across development.

In mice, the final form of the dendritic tree is largely established by the first 2 wk of postnatal life, well prior to adolescence (17). Afterward, large-scale structures are remarkably stable, although small degrees of growth have been observed in L2/3 pyramidal neurons using long-term imaging approaches (18). Results from genetic knockdown studies in vivo suggest that mature cortical neurons retain the ability for growth but typically remain stable in size due to competing inhibitory pathways (17). Our data support this notion, as we show that apical

dendrites are capable of continued growth across adolescence in WT mice, albeit only a modest increase.

Our data from the *Kalrn*-PT mice suggest that emergence of a structural phenotype results not from failure of normal dendritic growth early in development but, rather, regression of the existing dendrites during adolescence. Specifically, the dendritic arbors in the *Kalrn*-PT mice appear to reach a normal final form in preadolescence, indicating that they undergo the rapid growth phase early in development without interference. However, structural deficits emerge across adolescence and are evident by early adulthood, suggesting a pathological disruption of normal developmental processes. Our data show that apical arbors fail to achieve modest continued growth across adolescence. Since they achieve a normal preadolescent form, it is unlikely that this failure to grow is a deficit in a growth pathway but, rather, is more likely attributable to increased activity in a regression pathway. This is supported by our observation that the basilar arbors regress across adolescence in *Kalrn*-PT mice whereas wild-type basilar arbors remain stable, again suggesting that *Kalrn*-PT confers a pathological increase in dendritic regression emergent across adolescence.

Previous data suggest a role for MAIs in regulating cytoskeletal dynamics and neurite length (45, 76–78). Thus, an important consideration is whether the adolescent onset of dendritic regression seen in our *Kalrn*-PT mice reflects enhanced OMGp signaling as seen in our in vitro studies. OMGp is expressed both on the membranes of oligodendrocytes as well as by mature neurons (40, 46). In mice, OMGp increases from P0 onwards, reaching maximum levels in adulthood (40). This developmental patterning of expression poises OMGp to play a key role across adolescence and into adulthood, likely functioning in normal dendritic growth restriction and stabilization. The synergistic interaction of increasing expression of OMGp across normal adolescence with a genetic vulnerability (in this case, *Kalrn*-PT) that enhances RhoA signaling downstream of NGR1 would then result in dendritic regression emerging by early adulthood.

Dendrites, Auditory Processing Integrity, and SZ. Dendritic length and branching determine a PCs receptive field (11, 12), help to segment computational compartments (13), and contribute substantially to how the received signals are integrated and transmitted to the cell body (14, 15). Dendrites in early adult *Kalrn*-PT animals demonstrate less length and complexity than their wild-type counterparts. To determine any effect on spines as a result of this pathology, we measured dendritic spine density per unit length of dendrite as well as a measure of presumptive spine objects using identification of dual-reactive spinophilin/phalloidin puncta, a measure previously shown to overlap with dendritic spines in vivo (59). Notably, this pathology results only in reduced dendritic spine tissue density due to the dendritic arbor changes themselves, as there was no accompanying change in spine density per unit length of dendrite. Postmortem findings in SZ similarly show a reduction in dendritic length and in dendritic spine tissue density (10). Dendritic spines receive the majority of glutamatergic synapses in the cortex. In the auditory cortex, most of the spines receive narrowly tuned frequency inputs and, as such, serve to spatially and biochemically segregate frequency tuning (79). The reduced numbers of spines would therefore be hypothesized to impair frequency discrimination and processing of auditory information, ultimately producing the auditory sensory processing impairments seen in SZ (5).

One of the most reproducible electroencephalogram findings in SZ is decreased amplitude of the mismatch negativity response and change in sound properties, such as silent gaps in noise (6, 80). Gap detection, which in rodents can be indirectly assessed via the inhibition of the acoustic startle response when a prepulse, consisting of a gap in a noise background, is detected, requires integrity of the auditory cortex. In contrast, noise-PPI reflects sensorimotor gating that relies on subcortical circuitry and can still be elicited when the cortex is silenced or lesioned (61, 62). We found that *Kalrn*-PT mice have reduced inhibition specific to short gap duration (4 ms in *Kalrn*-WT versus 20 ms in *Kalrn*-PT), indicative of an impairment in gap

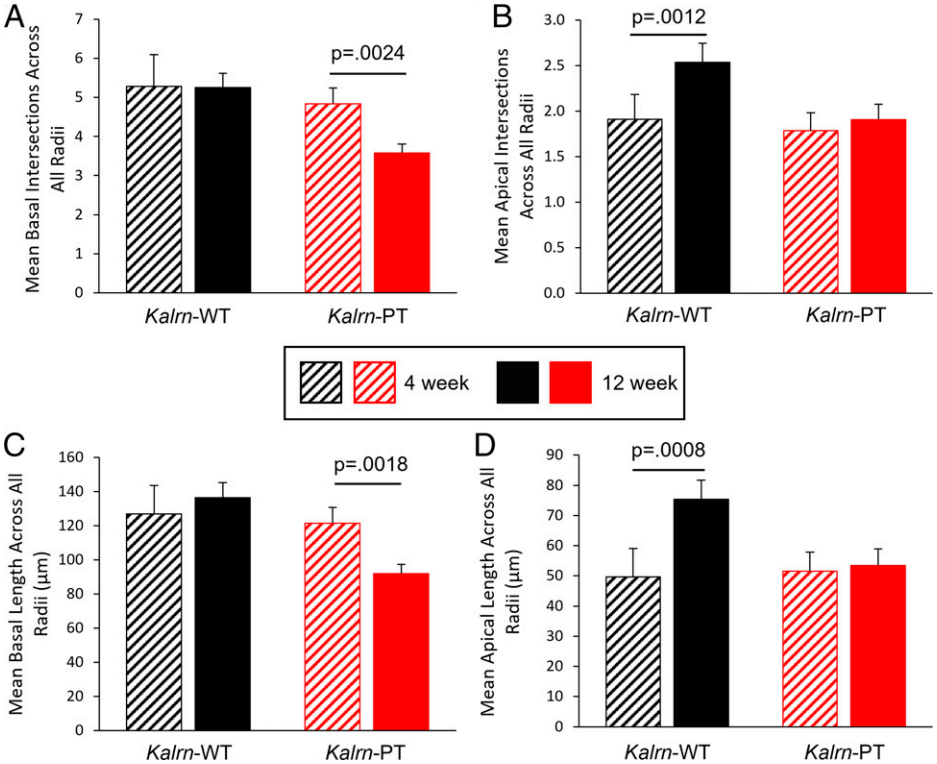

Fig. 6. Changes in dendritic architecture across adolescence in *Kalrn*-WT and *Kalrn*-PT mice. (*A*) Mean basilar intersections across age groups demonstrate a significant regression across adolescence in the *Kalrn*-PT animals, with no change in *Kalrn*-WT animals. (*B*) Mean apical intersections across age groups shows a significant increase in complexity in *Kalrn*-WT animals, with no change in *Kalrn*-PT animals. (*C*) Mean basilar length across age groups shows a regression across adolescence in *Kalrn*-PT, but not *Kalrn*-WT, animals. (*D*) Mean apical length increases across adolescence in *Kalrn*-WT animals, with no change in *Kalrn*-PT animals. All datasets shown are from the previously defined cohorts, $n = 10$ animals/genotype. Data are displayed ± SEM. *P* values for individual arbor analyses are displayed above the graphs. Total arbor statistics shown are $^*P < 0.1$.

detection threshold. The inability to detect short gap durations suggests a very specific auditory information processing deficit. These findings provide a useful model in which structural impairments within auditory cortical neurons are associated with a specific auditory cortical processing deficit rather than a global impairment in sensorimotor gating.

Conceptualizing Genetic Vulnerabilities across Normative Development. The data presented within show that *Kalrn*-PT induces adolescent-onset dendritic regression via enhancement of NGR1 signaling to RhoA. These findings contribute to the expanding understanding of how alterations in the dual GEFs Kalirn, and, its paralog, Trio contribute to risk for SZ. Moreover, we provide a model for how a mild genetic vulnerability may interact with the normal developmental timeline such that pathology only emerges in or after adolescence. This interplay between genetic susceptibility and normal adolescent development, both of which possess inherent interindividuality variability, may predict the heterogeneity seen in phenotypes in human neuropsychiatric disease.

Methods

CRISPR/Cas9.

CRISPR reagent production. A truncated sgRNA (81) targeting *KALRN* was designed using CRISPR Design Tool (82). An sgRNA specific forward primer and a common overlapping reverse PCR primer (*SI Appendix*, Table S1) were used to generate a T7 promoter containing sgRNA template as described (83). This DNA template was transcribed in vitro using a MEGAshortscript Kit (Ambion). The Cas9 mRNA was prepared using a MEGAshortscript kit (Ambion) as described (84). Following synthesis, the sgRNAs and Cas9 mRNA were purified using the MEGAclear Kit (Ambion), ethanol precipitated, and resuspended in DEPC-treated water. A single-stranded 130 nucleotide DNA repair template ("repair oligo," reference *SI Appendix*, Table S1) harboring the knock-in sequence (C→A) as well as a silent mutation (C→T) introducing a unique Hinf1 restriction site was purchased as polyacrylamide gel electrophoresis purified Ultramer DNA (Integrated DNA Technologies). Final codon change was from CCC (wild-type) to ACT (knock-in). The oligo was complementary to the nontarget strand (85).

Knock-in mouse production. sgRNA (50 ng/μL), Cas9 mRNA (75 ng/μL), and the repair oligo (100 ng/μL) were mixed and injected into the cytoplasm of C57BL/6J one-cell mouse embryos as described (84).

Mouse genotype analysis. Mice were genotyped by PCR amplification (reference *SI Appendix*, Table S1 for primer sequences, KALF2 and KALR2) followed by restriction digestion with Hinf1 (FastDigest) to produce PCR amplicons that were either 302 base pairs (bp) (wild-type) or 138 bp + 164 bp (knock-in). Undigested PCR amplicons of founder and all F1 offspring were also analyzed by Sanger sequencing.

Off-target analysis. The top 18 predicted off-target sites (*SI Appendix*, Table S2) using Cas9 Online Designer software (86) were analyzed by PCR amplification followed by Sanger sequencing.

Golgi.

Tissue generation. Cohorts of mice were killed at age 12 wk ± 3 d and 4 wk ± 3 d. These ages correspond in general to young adulthood and preadolescence, respectively, in mice (87, 88). Age-matched cohorts that included males and females of the two genotypes of interest (wild-type and homozygous *Kalrn-PT*) were processed together throughout. Vaginal cytology was collected on all early adult female mice at the time of killing. Mice were killed by lethal CO_2 inhalation followed by decapitation. Golgi staining was performed using the FD Rapid GolgiStain Kit (FD Neurotechnologies, Inc) according to manufacturer's instructions.

For the analysis of spine density, we chose to focus on proximally arising secondary apical dendrites for several reasons: 1) we found significant reductions in dendritic length and complexity in apical arbors, demonstrating that *Kalrn-PT* is exerting effects on apical dendrites; and 2) the focus on secondary apical dendrites allowed us to institute highly consistent criteria for selection. The latter is particularly important given that spine density is known to vary depending on distance from the soma.

Auditory cortex mapping. Animals were coded so that the experimenter remained blind to genotype throughout. Using Slidebook 6.0 (Intelligent Imaging Innovations) software, a 4× montage image of a Golgi-stained coronal section was obtained and aligned with the corresponding Nissl plate containing A1 (which spans ∼2.18 to 3.64 mm posterior to Bregma and 4.5 mm lateral to the midline) in the mouse brain atlas. An average of four sections per animal contained A1. An outline of A1 was drawn at 4× magnification, using the dorsal extent of the posterior commissure as an anatomical fiduciary (*SI Appendix*, Fig. S5). Within A1, deep layer 3 was defined as 30 to 50% of the distance between the pial surface and white matter border (*SI Appendix*, Fig. S5), and sampling of PCs was performed as described below (see *Immunohistochemistry*).

Immunohistochemistry. An additional cohort of mice aged 12 wk ± 3 d was generated. Mice were killed as above (see *Golgi, Tissue Generation*); the brains were sagittally hemisectioned, and the left hemisphere was fixed in 4% paraformaldehyde overnight at 4 °C. Tissue was then transferred to 18% sucrose solution for sectioning on a cryostat. The cerebellum was removed, and the tissue block was mounted and cut rostral to caudal at 40-μm thick sections. Every eighth section was pulled for Nissl staining. Nissl sections were used for guidance to determine tissue sections that contained auditory cortex. Detailed methods from our laboratory for auditory cortex mapping are found in ref. 9. One section containing auditory cortex per animal was used for immunohistochemistry (IHC).

In order to visualize dual-labeled immunoreactive puncta, we used two markers in combination: a rabbit polyclonal antibody directed against spinophilin (Millipore AB5669) at a dilution of 1:1,500. The second was the f-actin binding mushroom toxin phalloidin (Invitrogen A12380) conjugated to Alexa Fluor 568. Spinophilin is highly enriched in spine heads (56, 58). Phalloidin binds f-actin, which is also highly enriched in dendritic spines (57).

Please see *SI Appendix* for expanded *Methods*.

Data Availability. All study data are included in the article and/or supporting information.

ACKNOWLEDGMENTS. Funding was received from the following: MH071533 grant (R.A.S.), National Association for Research on Schizophrenia and Depression (NARSAD) Distinguished Investigator Grant from the Brain & Behavior Research Foundation Award (R.A.S.), MH118513-01 grant (M.J.G.), MH071316 grant (P.P.), MH097216 grant (P.P.), AA020889 grant (G.E.H.), R56AG058593 grant (Z.P.W.), and NARSAD Young Investigator Award (Z.P.W.).

1. P. V. Gejman, A. R. Sanders, J. Duan, The role of genetics in the etiology of schizophrenia. *Psychiatr. Clin. North Am.* **33**, 35–66 (2010).
2. M. F. Green, What are the functional consequences of neurocognitive deficits in schizophrenia? *Am. J. Psychiatry* **153**, 321–330 (1996).
3. M. F. Green, Cognitive impairment and functional outcome in schizophrenia and bipolar disorder. *J. Clin. Psychiatry* **67**, e12 (2006).
4. M. L. Thomas *et al.*, Modeling deficits from early auditory information processing to psychosocial functioning in schizophrenia. *JAMA Psychiatry* **74**, 37–46 (2017).
5. D. C. Javitt, R. A. Sweet, Auditory dysfunction in schizophrenia: Integrating clinical and basic features. *Nat. Rev. Neurosci.* **16**, 535–550 (2015).
6. P. T. Michie, What has MMN revealed about the auditory system in schizophrenia? *Int. J. Psychophysiol.* **42**, 177–194 (2001).
7. J. DeFelipe, I. Fariñas, The pyramidal neuron of the cerebral cortex: Morphological and chemical characteristics of the synaptic inputs. *Prog. Neurobiol.* **39**, 563–607 (1992).
8. D. A. Lewis, R. A. Sweet, Schizophrenia from a neural circuitry perspective: Advancing toward rational pharmacological therapies. *J. Clin. Invest.* **119**, 706–716 (2009).
9. M. A. Shelton *et al.*, Loss of microtubule-associated protein 2 immunoreactivity linked to dendritic spine loss in schizophrenia. *Biol. Psychiatry* **78**, 374–385 (2015).
10. C. E. Moyer, M. A. Shelton, R. A. Sweet, Dendritic spine alterations in schizophrenia. *Neurosci. Lett.* **601**, 46–53 (2015).
11. G. M. Shepherd, A. Stepanyants, I. Bureau, D. Chklovskii, K. Svoboda, Geometric and functional organization of cortical circuits. *Nat. Neurosci.* **8**, 782–790 (2005).
12. Q. Wen, D. B. Chklovskii, A cost-benefit analysis of neuronal morphology. *J. Neurophysiol.* **99**, 2320–2328 (2008).
13. J. Cichon, W. B. Gan, Branch-specific dendritic Ca(2+) spikes cause persistent synaptic plasticity. *Nature* **520**, 180–185 (2015).
14. A. Losonczy, J. K. Makara, J. C. Magee, Compartmentalized dendritic plasticity and input feature storage in neurons. *Nature* **452**, 436–441 (2008).
15. N. Spruston, Pyramidal neurons: Dendritic structure and synaptic integration. *Nat. Rev. Neurosci.* **9**, 206–221 (2008).
16. Y. N. Jan, L. Y. Jan, Branching out: Mechanisms of dendritic arborization. *Nat. Rev. Neurosci.* **11**, 316–328 (2010).
17. D. K. Chow *et al.*, Laminar and compartmental regulation of dendritic growth in mature cortex. *Nat. Neurosci.* **12**, 116–118 (2009).
18. A. Holtmaat, K. Svoboda, Experience-dependent structural synaptic plasticity in the mammalian brain. *Nat. Rev. Neurosci.* **10**, 647–658 (2009).
19. J. P. Bourgeois, P. S. Goldman-Rakic, P. Rakic, Synaptogenesis in the prefrontal cortex of rhesus monkeys. *Cereb. Cortex* **4**, 78–96 (1994).
20. P. R. Huttenlocher, Synaptic density in human frontal cortex—Developmental changes and effects of aging. *Brain Res.* **163**, 195–205 (1979).

21. D. A. Lewis, Development of the prefrontal cortex during adolescence: Insights into vulnerable neural circuits in schizophrenia. *Neuropsychopharmacology* **16**, 385–398 (1997).
22. T. Paus, M. Keshavan, J. N. Giedd, Why do many psychiatric disorders emerge during adolescence? *Nat. Rev. Neurosci.* **9**, 947–957 (2008).
23. M. S. Keshavan, S. Anderson, J. W. Pettegrew, Is schizophrenia due to excessive synaptic pruning in the prefrontal cortex? The Feinberg hypothesis revisited. *J. Psychiatr. Res.* **28**, 239–265 (1994).
24. A. L. Sporn *et al.*, Progressive brain volume loss during adolescence in childhood-onset schizophrenia. *Am. J. Psychiatry* **160**, 2181–2189 (2003).
25. P. R. Huttenlocher, A. S. Dabholkar, Regional differences in synaptogenesis in human cerebral cortex. *J. Comp. Neurol.* **387**, 167–178 (1997).
26. J. A. Markham, S. E. Mullins, J. I. Koenig, Periadolescent maturation of the prefrontal cortex is sex-specific and is disrupted by prenatal stress. *J. Comp. Neurol.* **521**, 1828–1843 (2013).
27. J. P. Bourgeois, P. Rakic, Changes of synaptic density in the primary visual cortex of the macaque monkey from fetal to adult stage. *J. Neurosci.* **13**, 2801–2820 (1993).
28. L. Luo, Actin cytoskeleton regulation in neuronal morphogenesis and structural plasticity. *Annu. Rev. Cell Dev. Biol.* **18**, 601–635 (2002).
29. I. Kushima *et al.*, Resequencing and association analysis of the KALRN and EPHB1 genes and their contribution to schizophrenia susceptibility. *Schizophr. Bull.* **38**, 552–560 (2012).
30. T. A. Russell *et al.*, A schizophrenia-linked KALRN coding variant alters neuron morphology, protein function, and transcript stability. *Biol. Psychiatry* **83**, 499–508 (2018).
31. G. Ahnert-Hilger *et al.*, Differential effects of Rho GTPases on axonal and dendritic development in hippocampal neurones. *J. Neurochem.* **90**, 9–18 (2004).
32. Y. Pilpel, M. Segal, Activation of PKC induces rapid morphological plasticity in dendrites of hippocampal neurons via Rac and Rho-dependent mechanisms. *Eur. J. Neurosci.* **19**, 3151–3164 (2004).
33. A. Y. Nakayama, M. B. Harms, L. Luo, Small GTPases Rac and Rho in the maintenance of dendritic spines and branches in hippocampal pyramidal neurons. *J. Neurosci.* **20**, 5329–5338 (2000).
34. A. W. Harrington *et al.*, The role of Kalirin9 in p75/nogo receptor-mediated RhoA activation in cerebellar granule neurons. *J. Biol. Chem.* **283**, 24690–24697 (2008).
35. T. Yamashita, K. L. Tucker, Y. A. Barde, Neurotrophin binding to the p75 receptor modulates Rho activity and axonal outgrowth. *Neuron* **24**, 585–593 (1999).
36. M. S. Chen *et al.*, Nogo-A is a myelin-associated neurite outgrowth inhibitor and an antigen for monoclonal antibody IN-1. *Nature* **403**, 434–439 (2000).
37. A. Zemmar *et al.*, Oligodendrocyte- and neuron-specific Nogo—A restrict dendritic branching and spine density in the adult mouse motor cortex. *Cereb. Cortex* **28**, 2109–2117 (2018).
38. G. Novak, D. Kim, P. Seeman, T. Tallerico, Schizophrenia and Nogo: Elevated mRNA in cortex, and high prevalence of a homozygous CAA insert. *Brain Res. Mol. Brain Res.* **107**, 183–189 (2002).
39. A. J. Deo *et al.*, Increased expression of Kalirin-9 in the auditory cortex of schizophrenia subjects: Its role in dendritic pathology. *Neurobiol. Dis.* **45**, 796–803 (2012).
40. A. G. Boghdadi, L. Teo, J. A. Bourne, The involvement of the myelin-associated inhibitors and their receptors in CNS plasticity and injury. *Mol. Neurobiol.* **55**, 1831–1846 (2018).
41. V. Gil *et al.*, Developmental expression of the oligodendrocyte myelin glycoprotein in the mouse telencephalon. *Cereb. Cortex* **20**, 1769–1779 (2010).
42. R. D. Fritz *et al.*, A versatile toolkit to produce sensitive FRET biosensors to visualize signaling in time and space. *Sci. Signal.* **6**, rs12 (2013).
43. Y. Zhao *et al.*, Amyloid beta peptides block new synapse assembly by nogo receptor-mediated inhibition of T-type calcium channels. *Neuron* **96**, 355–372.e6 (2017).
44. Z. P. Wills *et al.*, The nogo receptor family restricts synapse number in the developing hippocampus. *Neuron* **73**, 466–481 (2012).
45. V. Kottis *et al.*, Oligodendrocyte-myelin glycoprotein (OMgp) is an inhibitor of neurite outgrowth. *J. Neurochem.* **82**, 1566–1569 (2002).
46. A. A. Habib *et al.*, Expression of the oligodendrocyte-myelin glycoprotein by neurons in the mouse central nervous system. *J. Neurochem.* **70**, 1704–1711 (1998).
47. A. Williams, J. Henao-Mejia, R. A. Flavell, Editing the mouse genome using the CRISPR-Cas9 system. *Cold Spring Harb. Protoc.* **2016**, pdb.top087536 (2016).
48. R. C. Johnson, P. Penzes, B. A. Eipper, R. E. Mains, Isoforms of kalirin, a neuronal Dbl family member, generated through use of different 5'- and 3'-ends along with an internal translational initiation site. *J. Biol. Chem.* **275**, 19324–19333 (2000).
49. P. Penzes, K. A. Jones, Dendritic spine dynamics—A key role for kalirin-7. *Trends Neurosci.* **31**, 419–427 (2008).
50. M. J. Gandal *et al.*, PsychENCODE Consortium, Transcriptome-wide isoform-level dysregulation in ASD, schizophrenia, and bipolar disorder. *Science* **362**, eaat8127 (2018).
51. R. A. Sweet *et al.*, Pyramidal cell size reduction in schizophrenia: Evidence for involvement of auditory feedforward circuits. *Biol. Psychiatry* **55**, 1128–1137 (2004).
52. R. A. Sweet, R. A. Henteleff, W. Zhang, A. R. Sampson, D. A. Lewis, Reduced dendritic spine density in auditory cortex of subjects with schizophrenia. *Neuropsychopharmacology* **34**, 374–389 (2009).
53. K. A. Dorph-Petersen *et al.*, Pyramidal neuron number in layer 3 of primary auditory cortex of subjects with schizophrenia. *Brain Res.* **1285**, 42–57 (2009).
54. B. C. McKinney *et al.*, Density of small dendritic spines and microtubule-associated-protein-2 immunoreactivity in the primary auditory cortex of subjects with schizophrenia. *Neuropsychopharmacology* **44**, 1055–1061 (2019).
55. B. H. Alexander *et al.*, Stable density and dynamics of dendritic spines of cortical neurons across the estrous cycle while expressing differential levels of sensory-evoked plasticity. *Front. Mol. Neurosci.* **11**, 83 (2018).
56. P. B. Allen, C. C. Ouimet, P. Greengard, Spinophilin, a novel protein phosphatase 1 binding protein localized to dendritic spines. *Proc. Natl. Acad. Sci. U.S.A.* **94**, 9956–9961 (1997).
57. F. Capani, M. H. Ellisman, M. E. Martone, Filamentous actin is concentrated in specific subpopulations of neuronal and glial structures in rat central nervous system. *Brain Res.* **923**, 1–11 (2001).
58. E. C. Muly, Y. Smith, P. Allen, P. Greengard, Subcellular distribution of spinophilin immunolabeling in primate prefrontal cortex: Localization to and within dendritic spines. *J. Comp. Neurol.* **469**, 185–197 (2004).
59. E. M. Parker, N. L. Kindja, C. E. J. Cheetham, R. A. Sweet, Sex differences in dendritic spine density and morphology in auditory and visual cortices in adolescence and adulthood. *Sci. Rep.* **10**, 9442 (2020).
60. M. Koch, The neurobiology of startle. *Prog. Neurobiol.* **59**, 107–128 (1999).
61. G. P. Bowen, D. Lin, M. K. Taylor, J. R. Ison, Auditory cortex lesions in the rat impair both temporal acuity and noise increment thresholds, revealing a common neural substrate. *Cereb. Cortex* **13**, 815–822 (2003).
62. J. R. Ison, K. O'Connor, G. P. Bowen, A. Bocirnea, Temporal resolution of gaps in noise by the rat is lost with functional decortication. *Behav. Neurosci.* **105**, 33–40 (1991).
63. M. J. Owen, M. C. O'Donovan, A. Thapar, N. Craddock, Neurodevelopmental hypothesis of schizophrenia. *Br. J. Psychiatry* **198**, 173–175 (2011).
64. M. Aceti *et al.*, Syngap1 haploinsufficiency damages a postnatal critical period of pyramidal cell structural maturation linked to cortical circuit assembly. *Biol. Psychiatry* **77**, 805–815 (2015).
65. A. J. Koleske, Molecular mechanisms of dendrite stability. *Nat. Rev. Neurosci.* **14**, 536–550 (2013).
66. P. Mandela *et al.*, Kalrn plays key roles within and outside of the nervous system. *BMC Neurosci.* **13**, 136 (2012).
67. S. E. Newey, V. Velamoor, E. E. Govek, L. Van Aelst, Rho GTPases, dendritic structure, and mental retardation. *J. Neurobiol.* **64**, 58–74 (2005).
68. G. J. Ramakers, Rho proteins, mental retardation and the cellular basis of cognition. *Trends Neurosci.* **25**, 191–199 (2002).
69. A. Sadybekov, C. Tian, C. Arnesano, V. Katritch, B. E. Herring, An autism spectrum disorder-related de novo mutation hotspot discovered in the GEF1 domain of Trio. *Nat. Commun.* **8**, 601 (2017).
70. C. Remmers, R. A. Sweet, P. Penzes, Abnormal Kalirin signaling in neuropsychiatric disorders. *Brain Res. Bull.* **103**, 29–38 (2014).
71. T. D. Cannon *et al.*, North American Prodrome Longitudinal Study Consortium, Progressive reduction in cortical thickness as psychosis develops: A multisite longitudinal neuroimaging study of youth at elevated clinical risk. *Biol. Psychiatry* **77**, 147–157 (2015).
72. A. M. McIntosh *et al.*, Longitudinal volume reductions in people at high genetic risk of schizophrenia as they develop psychosis. *Biol. Psychiatry* **69**, 953–958 (2011).
73. D. Sun *et al.*, Progressive brain structural changes mapped as psychosis develops in 'at risk' individuals. *Schizophr. Res.* **108**, 85–92 (2009).
74. G. Gasiunas, R. Barrangou, P. Horvath, V. Siksnys, Cas9-crRNA ribonucleoprotein complex mediates specific DNA cleavage for adaptive immunity in bacteria. *Proc. Natl. Acad. Sci. U.S.A.* **109**, E2579–E2586 (2012).
75. M. Jinek *et al.*, A programmable dual-RNA-guided DNA endonuclease in adaptive bacterial immunity. *Science* **337**, 816–821 (2012).
76. A. Mingorance-Le Meur, B. Zheng, E. Soriano, J. A. del Río, Involvement of the myelin-associated inhibitor Nogo-A in early cortical development and neuronal maturation. *Cereb. Cortex* **17**, 2375–2386 (2007).
77. L. Montani *et al.*, Neuronal Nogo-A modulates growth cone motility via Rho-GTP/LIMK1/cofilin in the unlesioned adult nervous system. *J. Biol. Chem.* **284**, 10793–10807 (2009).
78. L. McKerracher *et al.*, Identification of myelin-associated glycoprotein as a major myelin-derived inhibitor of neurite growth. *Neuron* **13**, 805–811 (1994).
79. X. Chen, U. Leischner, N. L. Rochefort, I. Nelken, A. Konnerth, Functional mapping of single spines in cortical neurons in vivo. *Nature* **475**, 501–505 (2011).
80. R. Näätänen, S. Pakarinen, T. Rinne, R. Takegata, The mismatch negativity (MMN): Towards the optimal paradigm. *Clin. Neurophysiol.* **115**, 140–144 (2004).
81. Y. Fu, J. D. Sander, D. Reyon, V. M. Cascio, J. K. Joung, Improving CRISPR-Cas nuclease specificity using truncated guide RNAs. *Nat. Biotechnol.* **32**, 279–284 (2014).
82. P. D. Hsu *et al.*, DNA targeting specificity of RNA-guided Cas9 nucleases. *Nat. Biotechnol.* **31**, 827–832 (2013).
83. A. R. Bassett, C. Tibbit, C. P. Ponting, J. L. Liu, Highly efficient targeted mutagenesis of *Drosophila* with the CRISPR/Cas9 system. *Cell Rep.* **4**, 220–228 (2013).
84. Y. A. Blednov *et al.*, Mutation of the inhibitory ethanol site in $GABA_A$ ρ1 receptors promotes tolerance to ethanol-induced motor incoordination. *Neuropharmacology* **123**, 201–209 (2017).
85. C. D. Richardson, G. J. Ray, M. A. DeWitt, G. L. Curie, J. E. Corn, Enhancing homology-directed genome editing by catalytically active and inactive CRISPR-Cas9 using asymmetric donor DNA. *Nat. Biotechnol.* **34**, 339–344 (2016).
86. D. Guo *et al.*, Online high-throughput mutagenesis designer using scoring matrix of sequence-specific endonucleases. *J. Integr. Bioinform.* **12**, 35–48 (2015).
87. W. Kilb, Development of the GABAergic system from birth to adolescence. *Neuroscientist* **18**, 613–630 (2012).
88. C. E. Moyer *et al.*, Developmental trajectories of auditory cortex synaptic structures and gap-prepulse inhibition of acoustic startle between early adolescence and young adulthood in mice. *Cereb. Cortex* **26**, 2115–2126 (2016).
89. J. G. Turner *et al.*, Gap detection deficits in rats with tinnitus: A potential novel screening tool. *Behav. Neurosci.* **120**, 188–195 (2006).